UNIVERSITY OF CALIFORNIA,
IRVINE

Simulation of Protoacoustics for FLASH Proton Dosimetry

THESIS

submitted in partial satisfaction of the requirements
for the degree of

MASTER OF SCIENCE

in Biomedical Engineering

by

Kaitlyn Kim

Thesis Committee:
Professor Liangzhong Xiang, Chair
Professor Zhongping Chen
Professor Lydia Min-Ying Su

2024

TABLE OF CONTENTS

LIST OF FIGURES

LIST OF TABLES

ACKNOWLEDGEMENTS

I would like to first express my sincerest gratitude to my advisor Dr. Liangzhong Xiang for the resources, tools, guidance, and support through this journey. Through his help and encouragement, I was able to grow and accomplish the skills that I have for this Masters thesis. I would also like to thank my committee members, Dr. Zhongping Chen and Dr. Lydia Min-Ying Su for their time and agreeing to serve on my committee.

I would also like to thank everyone in the TRUE lab for their help throughout my time. Without the help of my fellow lab members, I would not be where I am today. In particular, I'd like to thank Dr. Prabodh Kumar Pandey for helping me through simulation works and understanding the toolboxes necessary for completing this work. I'm also thankful towards our collaborators at OUHSC, Dr. Yong Chen and Gilberto Gonzalez for their unwavering support and contributions.

Lastly, I would like to thank all of my friends and family who have been there every step of the way.

ABSTRACT OF THE THESIS

Simulation of Protoacoustics for FLASH Proton Dosimetry
by

Kaitlyn Kim

Master of Science in Biomedical Engineering

University of California, Irvine, 2024

Professor Liangzhong Xiang, Chair

This thesis introduces the novel concepts of FLASH proton therapy and the use of Protoacoustics for *in vivo* dosimetry. FLASH proton therapy applies ultra-high dose rates to radiation therapy, which is beneficial in tissue sparing compared to conventional radiation therapy. By combining this characteristic with the elusive Bragg peak found in proton therapy, a highly effective therapy is formed. However, there is a need for a dosimeter that can accurately pinpoint and quantify the dose. In the text, current dosimeters are discussed as well as the trade-offs, leading into the significance of protoacoustics. Protoacoustics, which takes the concepts of radiation acoustics, is investigated through multiple simulation works, specifically in the context of FLASH proton therapy. Using the k-Wave toolbox in MATLAB, the protoacoustic signal amplitude was compared to changes in first the dose per pulse, then in pulsewidth. The relationship between the parameters were investigated and protoacoustic reconstructions were performed as well. The novel concept of spatially fractioned radiation therapy (SFRT) was also investigated in the form of Lattice Radiation Therapy (LRT) through a multibeam spot simulation. 3D reconstructions with varied pulse widths were observed for the spatial resolution and the feasibility of 3D imaging with protoacoustics.

CHAPTER 1: INTRODUCTION

The American Cancer Society states that cancer results in the death of over a half million of people globally each year, making it stand as the second leading cause of deaths[1].One of the major treatment modalities is radiation therapy, which has been developed and clinically applied for nearly a century[2]. Radiation therapy applies high radiation dosage for the purpose of killing the cancer cells and shrinking tumors. This type of treatment can be used for many different types of tumors as it works by damaging the DNA of the cancer cells[3]. Although radiation therapy has various benefits**,** the toxicity and harm it provides to the surrounding healthy tissues in a patient's body can sometimes outweigh the good. Because of this, there is a push towards using proton radiation.

Proton Therapy

Proton therapy was first introduced in 1954 by Lawrence et al. at the University of California Lawrence Berkeley Laboratory[4]. The main reason for the use of protons was due to its unique feature, where the deposited energy will primarily be focused into a single point, near the end of the beam's range. This distribution is known as the Bragg peak, which was discovered by Sir William Henry Bragg in 1904[5]. The discovery of the Bragg peak in proton beams revolutionized radiation therapy, as it allowed for a way to maximize the dose into a single location, rather than having radiation severely impact the surrounding organs and tissues. However, the improvements do not stop there. In the 1970s, experiments were conducted, which investigated how high dose rates of radiation differ from conventional dose rates on cells[6]. The reports showed a differential response between the two, paving a road towards a

new research path. Since then, significant strides have been taken towards applying this high dose rate into proton therapy, which is popularly coined as "FLASH" proton therapy.

FLASH proton therapy

FLASH proton therapy has become of such high interest due to its tissue-sparing properties[7]. Clinical results have shown FLASH to be just as effective as conventional dose rate treatment, but with far shorter delivery times[8]. Although there are still debates towards the exact definition of FLASH, the more agreed upon statement shown in literature is dose rates higher than 40 Gy/s, which is 400 times greater than conventional radiation dose rates (~0.01 – 0.4 Gy/s)[9,10]. The requirements for FLASH is ultimately a combination between the dose, dose rate, repetition rate, and the number of pulses that are being used. The biological side of FLASH is also in debate and how it provides its features of tissue sparing[11,12]. One primary idea is that oxygen depletion occurs and acts almost as hypoxia in normal tissue[13]. Oxygen not coming across into the normal tissue will cause the free radicals to not react with oxygen, which keeps the damaging peroxyl radicals from forming. The result of this is the increased resistance to radiation in the normal tissue. However, as mentioned before, this is simply one of the multiple ideas that have been mentioned for FLASH.

Initial experiments were completed in 2014, followed by various more studies displaying the legitimacy of FLASH in different tissue types[14]. Although many of the experiments displayed the use of electron therapy, there is still interest in using the same principle with proton due to their similarities in biologic effectiveness. The effects of FLASH proton therapy have been studied *in vitro* with successful results using human lung fibroblasts and comparing the outcome with a dose rate of 0.05 Gy/s and 100 Gy/s[15]. The results of this study showed a

decrease in senescent cells when using the FLASH (100 Gy/s) dose rate compared to the conventional (0.05 Gy/s) along with a decrease in TGF-β expression. There have also been multiple animal studies in mice specifically comparing FLASH and conventional dose rates[16]. There was tissue sparing that could be observed with FLASH with improved survival for the mice, showing the success that FLASH proton therapy had.

SFRT

Proton therapy has also evolved over recent years to improve the efficacy through many different techniques. One particular technique which has been emerging in the field is known as spatially fractioned radiation therapy (SFRT)[17]. SFRT is a concept initially introduced in the 20th century for the potential of tissue sparing during radiation therapy. In this particular technique, there are alternating regions for high dose (peaks) and low dose (valleys), which is created by segmenting the irradiation field into multiple narrow beamlets that are separated with small gaps[18]. SFRT can be split into four different types, primarily based on the arrangement and size of the beams: GRID-RT, lattice RT(LRT), minibeam RT, and microbeam RT. GRID-RT and LRT focus on centimeter-scale beamlets, and the primary difference between these two techniques is that LRT gives rise to a 3D configuration. The rise of LRT gives more flexibility in the sphere of SFRT, as there is much higher customization in the dose distributions of the peaks-to-valleys[19]. Alongside the growing interest in LRT and its use already in clinical trials, It's essential to have an imaging technique for real-time monitoring of GRID therapy during treatment.

Current Dosimeters

When conducting radiation therapy, the use of dosimeters is imperative, as the amount of exposure to the ionizing radiation should be monitored as closely as possible. Many tools have been developed and used for proton therapy and have also been used for FLASH specifically. For dosimetry tools, several aspects need to be considered. The accuracy of the readout is important, as well as the spatial and temporal resolution, and the dose-rate independence[20].

Dose-rate is one characteristic that will need to be heavily considered, particularly as the values between conventional radiation therapy and FLASH differ significantly. As FLASH rates are considered to be greater than 40 Gy/s, dosimeters that have the capabilities of measuring in these magnitudes will be necessary. Problems that typically arise include saturation as well as non-linear responses[21]. Spatial resolution is another characteristic that should be observed for finding the ideal dosimeter in FLASH. Ideally, detectors that have a spatial resolution less than 1 mm is wanted, but it's possible that a much finer resolution may be needed in the future[22]. As proton therapy is evolving overall, new types of techniques are being adapted and being used in the clinic, including changing the complexity of the beams. For concepts, such as Microbeam Radiation Therapy (MRT), which has been shown to have FLASH capabilities, the smaller resolution will be required[23]. Temporal resolution is of interest as well. There is a need for dosimeters that can be able to provide readouts in real-time for high dose rates. Although many existing dosimeters have excellent readout, they lack the real-time readouts and are simply passive monitoring methods[24]. There are also a variety of other characteristics to consider, such as dynamic range and energy dependence. Ultimately, each dosimeter has its strengths in applying to these characteristics, which will be discussed further below.

In many cases, a charge-based dosimeter is used for detection. These types of dosimeters create ion pairs that can be collected and correlated to dose later. Ion chambers (IC) are an example of a charge-based dosimeter and is in fact one of the most common methods of dosimetry where it collects the charges from direct ionization. Specifically, when there is interaction of the proton particles, charged particles that generate electric current are produced within the chamber[20]. The electric current is directly proportional to the ion number, which gives the information regarding the delivered dose. Although ion chambers have been used in FLASH, one of the primary challenges behind this method is that a correction factor needs to be applied to correct for the ion-recombination[25–27]. There is also saturation to consider with ICs, particularly when such high dose rates are being used as well as poor temporal resolution (~ms), making them not ideal real-time dosimeters.

Chemical dosimeters have also been used for FLASH therapy. These types of dosimeters are ones that will have structural changes when irradiated. For instance, Fricke, or ferrous ammonium sulfate, detectors are a type of chemical dosimeter that will undergo oxidation of ferrous ions to ferric ions upon interaction of ionizing radiation[28]. The number of ferric ions that are produced is proportional to the amount of dose that is delivered. The optical density of the solution can then be measured for further quantification. However, this dosimeter will be sensitive to low dose-rates over time as the diffusion of ferrous ions occurs. Alanine detectors are also another common type of chemical dosimeter. Alanine is an amino acid that upon radiation, will form stable radicals. The concentration of the free radical is directly proportional to the absorbed dose. This concentration is determined using electron paramagnetic resonance technique[29]. Alanine has a very large dynamic range, between 2 Gy – 150 kGy. Despite this range, there is considerable uncertainty below the 2 Gy for alanine

dosimeters[30]. There is also the issue where real-time measurements are not possible with this detector.

Solid-state detectors are another commonly used type of dosimeter. These types of detectors include diodes and diamonds. The operation of these small sized detectors is similar to that of ICs because radiation produces electron-hole pairs that can be collected in both[20]. One particular example that many experts have been interested in are the ultra-thin silicon detectors, which have a thickness of less than 10 μm. They're attractive due to their high sensitivity and spatial resolution[31]. The only downside to this technology is that real-time measurements have not yet been implemented.

Luminescent dosimeters are another major type of dosimeter that has been investigated in FLASH purposes. These types of dosimeters use the generated optical photons in response to radiation to determine the dose. One example of this is thermoluminescence detectors (TLD). These detectors work by encapsulating electrons and holes between the valence and conduction band, which is completed due to the impurities[32]. Electrons will move during irradiation, and the dose is read by the emitted light intensity. This light is a result of heat triggered by electron-hole recombination, which causes visible photons. TLDs have been used with high dose rates in the past, but the biggest drawbacks with this dosimeter is that real-time measurements are not possible as well as beam monitoring[9].

Scintillators are another type of detector using certain materials that have high energy photon or charged particles, causing emission of optical photons. Scintillators can typically be broken up into either organic or inorganic[33]. Organic scintillators are typically aromatic hydrocarbon compounds while inorganic scintillators are single or poly-crystalline

materials with impurities as luminescent centers. These scintillators can typically complete both point or 2D/3D measurements with the assistance of a CCD camera[34].

Radiation Acoustics

The idea of radiation acoustics first came to light with Alexander Bell's photophone discovery over 125 years ago[35]. This marked the first demonstration of light generating and detecting sound. Initial studies after the forthcoming of this idea came around in the 50s and 60s, with studies that observed acoustic signal generation through ultrasound, electrons, and even measurements of electron pulse beams on various crystals[36].

Since then, further studies have been taking this principle, now more commonly known as the photoacoustic effect, for various biomedical purposes. One of those ideas includes photoacoustic imaging[37]. Photoacoustic (PA) imaging typically uses pulsed radiation waves on a nanosecond timescale and irradiates a sample, causing excitation of ultrasound waves[37–40]. The penetration depth of PA will depend on the wavelength that is used. The push for photoacoustic imaging over the last several decades is for several reasons. Compared to modalities, such as ultrasound, there is much greater tissue differentiation as well as specificity due to the optical absorption between different tissue types[39].

Since the introduction of radiation acoustics, there have been multiple imaging techniques that arose. In 2013, acoustic waves for computed tomography were first introduced as X-ray induced Acoustic Computed Tomography (XACT)[41]. Here, a point transducer was immersed into water, then rotated around the beam to form a 2D reconstruction of the beam shape. The results from the measurements showed a direct proportionality between the amplitude

and the deposited dose of the source. This discovery showed the potential for XACT and other radiation acoustic techniques for real-time *in vivo* dosimetry[41].

Ultimately, the principles behind radiation acoustics carry over regardless of the source used. The target is irradiated with a pulsed energy source, the energy deposition causes a local temperature rise, and during the diffusion process, the temperature will decrease[42]. This causes the thermoelastic expansion in the target, which is when there is a rapid heating and cooling cycle for expansion and contraction for pressure gradients.

Protoacoustics for FLASH

Protoacoustics, also known as ionoacoustics, is a novel and rapidly evolving technique stemming from radiation acoustics[43]. It unites the principles of thermoacoustic imaging mentioned above with cutting-edge proton therapy. Currently, within the field, there is a lack of in vivo non-invasive dosimetric technologies that can be used. However, this gap can be easily filled with protoacoustics. As the proton beam energy deposition produces a rise in local temperature, a pressure wave is formed, which can be traced down to a physical measurable signal related to this initial temperature increase[43].

The principles behind protoacoustics hinge on the interaction between protons and human tissues during radiation therapy. While protons are propelled into the body, they decelerate and deposit their energy, which prompts tissues to heat and subsequently expand[43,44]. The result of this expansion causes the emission of acoustic waves, which can be captured by ultrasound detectors and transformed into images. This information is significant in determining the location as well as the extent of interaction between the proton beam and tissues, serving as a real-time range verification tool during proton therapy. The accuracy

and precision of such a tool leads into the potential of minimizing damage to healthy tissues during cancer therapies.

Historically, the idea to use protoacoustics for clinical applications has been ongoing since 1979[45]. After initial advancements in the field around the 1980s, there was a moment of stagnation until the early 2000s with the introduction of new generation accelerator machines, such as the synchrocyclotron or laser-driven sources[46,47]. These short pulsed, high intensity beams favor protoacoustics heavily with the μs to ns pulses. This combined with the rapid advancements in ultrasound transducer technology has led into the heavy development towards protoacoustics.

The technology for protoacoustics has great potential in the medical imaging field with interest already being garnered by those in the scientific community as well as clinical practice. Protoacoustics is low cost, requiring just a transducer for measurements, and can be used without interference of the therapeutic beam. Compared to other dosimetry tools, there is also improved spatial resolution and submillimeter accuracy when measuring the proton range using the time of flight[48–55]. Although it is a newer technology that only has a handful of groups developing this concept, the rapid progress in advancing protoacoustics shows the potential it has for the future of medical imaging.

Transducer Types

Protoacoustic measurements have been completed in both point measurements and 2D imaging through the use of arrays. For the simplest types of measurements, a single acoustic transducer is used for A-line protoacoustic signal detection. Some of the earliest work that accomplishes this is in 1979 by Sulak et al. when acoustic signals were detected from a 150

MeV proton beam[45]. This was accomplished through the use of hydrophones in a water medium, where one captured signals between 1 KHz to 150 KHz, while the other detected up to 1 MHz. Other works using a hydrophone included one in 1991 using a 300 KHz hydrophone for acoustic signal detection in a proton source[47]. Although hydrophones are a strong tool for measurements, they require precise alignment for the high quality signal capturing and typically have low signal-to-noise ratio (SNR). The technology was further refined by Sueysa et al. in 2023 by introducing an optical hydrophone[56]. This device uses laser interferometry to detect low pressure signals from the proton beam and addresses the issues of signal reduction from misalignment.

There's also the use of conventional ultrasound transducers for detecting proton beams, such as those composed of lead zirconate titanate (PZT) or polyvinylidene fluoride (PVDF). In a study completed by Assmann et al., a PZT based transducer was used for measuring single proton pulses at 3.5 MHz and 10 MHz frequencies[57]. However, maintaining a low SNR was a challenge, similar to the conventional hydrophones. Studies done by Lascaud et al. used a PVDF transducer for detecting proton signals as low as 100 KHz with tungsten serving as the backing of the transducer for enhanced sensitivity[58]. Comparatively, PZT transducers display a higher detection sensitivity than PVDF-based transducers, although bandwidth is still an issue for the PZT. There is also the use of capacitive micromachined ultrasonic transducers (CMUTs), which have a wide bandwidth with no regarding or attenuation of the proton signal[59]. The 12 MHz CMUT prototype demonstrated is capable of signal detection of several KHz to MHz. Ultimately, there is still a necessity in continuation of researching an acoustic transducer capable of broad bandwidth and high detection sensitivity.

Although the single point measurement devices mentioned have been significant in demonstrating the potential for proton signal measurements, there are constraints in creating images unless a mechanical stage is used. Because of this, there is a push towards using transducer arrays for protoacoustic wave detection. Not only can this allow for image reconstruction, but real-time 3D measurements *in vivo* become a possibility with this new technology. Within Ionizing Radiation Acoustic Imaging (iRAI), a concept with a similar principle to protoacoustics by using an electron source, there has already been success in detecting thermoacoustic waves using a 2D matrix array[60]. Similarly, Bjegovic et al. displayed the use of 4D dosimetry for FLASH electron therapy using a 256-element matrix array. A rabbit cadaver was imaged in real-time with full volumetric view of the individual pulses[61]. In the realm of protoacoustics, there have not been any experimental studies utilizing an array transducer. However, multiple papers have explored the concept through simulation studies. One study showcased 3D protoacoustic imaging through the use of a matrix array[53]. In the study, dose reconstruction was completed using the array, and frequency characteristics from the protoacoustics signals were identified. Based on the promising results of such works, protoacoustic imaging is poised to take significant leaps towards 3D imaging and real-time *in vivo* dosimetry.

Signal Processing and Software Development

Although hardware has been advancing for protoacoustics, there is still the concern of low SNR for the protoacoustic measurements. Due to this, many techniques have been investigated to enhance the SNR, such as low-pass filters, wavelet noising, etc.[62]. Averaging and filtering prior to any processing of a protoacoustic signal is necessary for enhancing the

SNR , with wavelet filtering receiving more interest for its potential in the field[63,64]. There's also further research, which has shown the use of Savitzky-Golay filters to also be helpful in elevating the SNR significantly, especially when it comes to single pulse protoacoustic measurements[65].

After pre-processing and filtering the protoacoustic signal, visualization is a key step in protoacoustics. This is important for Bragg peak localization and dose information. For this purpose, many reconstruction algorithms have been developed over the years, drawing inspiration from photoacoustic reconstructions[66]. For instance, Kellenberger et al. used a modified back-projection algorithm as well as a model-based reconstruction to obtain protoacoustic images[67]. These reconstructions displayed the maximum intensity of a 20 MeV proton beam as well as the location of the Bragg peak. There have also been advancements made in the 3D dose distribution reconstruction algorithms for different types of machines, such as isochronous cyclotrons and synchrocyclotrons[68]. Another innovative approach in reconstruction includes numerical time-reversal, which uses transducer arrays to approximate thermoacoustic waves and reconstruct the acoustic source amplitude[69]. However, one of the common problems that occur from this reconstruction and others for protoacoustic imaging is the limited view problem, where the ultrasound transducer's view is too restricted. To tackle this problem, deep learning-based methods have been employed and a deep cascaded convolutional network (DC-CNN) has been explored[70]. In this particular study, 81 prostate cancer patients' treatment plans were used, and the dose calculations as well as PA simulations were completed through commercial software and k-Wave toolbox. This method was trained then used on patient samples using the reconstructed pressures and dose maps compared to ground truth data with various metrics. The overall results

showed improvements to the limited-view PA image quality with accurate pressure structures and high agreement between the derived doses and ground truth data[70]. The approach aimed to reconstruct high-quality radiation-induced pressures and obtain accurate 3D dosimetry from the PA signals from a matrix array for prostate proton therapy. All of the efforts listed have aided in improving the overall quality of protoacoustic signal collection and reconstruction so it can be used in the clinic.

Purpose of this paper

The completed study is the first simulation paper investigating the parameters of protoacoustics under FLASH therapy conditions. Due to the novelty of FLASH itself, there are many characteristics and guidelines that are not defined for this concept, especially as the primary contributing factors are not fully defined. Because of this, we have performed multiple simulations based on the dose per pulse and pulsewidth variation to fit within the FLASH regime in order to view the effects each parameter has on the protoacoustic signal amplitude. The concept of FLASH proton therapy is consistently evolving. One of the upcoming techniques includes the use of spatially fractioned radiation therapy (SFRT)[17]. Due to the growing interest of this topic, the reconstruction of specific cases were explored using protoacoustics.

CHAPTER 2. K-Wave/TOPAS Simulation

TOPAS Simulation

As this area of research is still a new concept with many physical limitations and barriers, the nature of this work is purely simulation-based. To begin, the proton pencil beam dose distributions were modeled. This initial step is completed using TOPAS (Toolkit for Particle Simulation) version 3.1.2. TOPAS is a simulation extension toolkit from Geant4, which is used for modeling x-ray and particle therapy[71]. Geant4 is known as a general kit for physics models, particularly with medical applications. However, the development of TOPAS has allowed for less programming knowledge and is more user friendly for easy configuration of medical physics simulations[72]. Using TOPAS, the material composition and beam parameters can be edited for obtaining proton beam range or stopping reported as reported in PSTAR database or NIST tables. In the simulations for this study proton beam spot sizes were set between 1.0 to 3.0 mm with several shifts in the X-Y plane position. To collect the dose deposition, a water phantom geometry was used. The dimensions for this water phantom were set to 8 cm x 8 cm x 30 cm with a 0.5 mm resolution per voxel. The 3D grid resolution used was set to 0.5 mm voxels. For the proton beam energies, a 200 MeV and 150 MeV beam were used. Upon obtaining the dose distributions from TOPAS as a table file, the simulated doses were sent to MATLAB for the next step of simulations in k-Wave. An example of the simulation in TOPAS and how the proton beams are created for each instance is shown in Figure 1. This particular figure shows one of the proton beam profiles used where 9 beamlets were heading towards a water phantom. The grid size for the voxel and dose collection were set to 1 mm^3. One million stories were set per beam to achieve sufficient statistics.

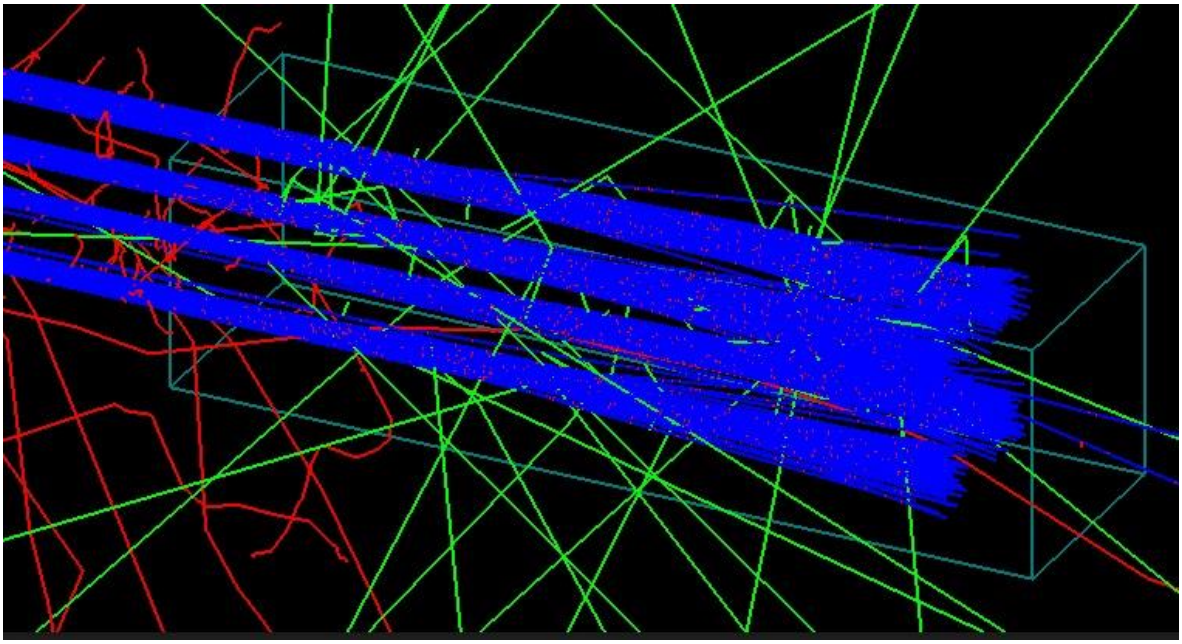

Figure 1. Simulation of the proton beam in TOPAS. The figure demonstrates the generation of the proton beam profile for the 150 MeV multibeam spot profile.

k-Wave Simulation

The physics behind protoacoustics can be likened to that of photoacoustics, and the initial acoustic pressure (P_0) can be related to dose deposition (D) through the following equation:

$$P_0 = \Gamma \rho D, \qquad (1)$$

Where Γ represents the Gruneisen coefficient and ρ is the density of water. The Gruneisen parameter is a dimensionless parameter, which is typically measured from isobaric thermal expansion or through photoacoustic spectroscopy[73]. Because of the similarities in physics, k-Wave toolbox in MATLAB was used for all simulation work completed. k-Wave is a

simulation and reconstruction toolbox that models photoacoustic wave fields[74]. Similarly, we were able to apply the toolbox for the use of modeling the protoacoustic wave fields in this particular study. Initial acoustic pressure was predefined using $\Gamma = 0.11$ and $\rho = 1000$ kg/m^3, which are measured values in distilled water[75,76].

Protoacoustic pressure intensity has been shown to be linearly dependent on the deposited dose. Because of the importance in linearity, it's also important that the simulation was modeled with some added complexity. The variable medium.BonA was added to the simulation work and compared to when this variable is not set to see if there is a difference in the response. The medium.BonA variable was set to 5, which is a common value used in soft tissue[77]. The comparison was done using the same dose per pulse and pulsewidth (20 cGy/pulse with 4 μs pulsewidth) and is shown in Figure 2. The difference between the two is negligible, meaning that regardless of the variable, linearity holds in the simulation. These results ultimately show that linearity will hold even within the FLASH regime for the simulation, which allows for further experimental exploration in protoacoustics.

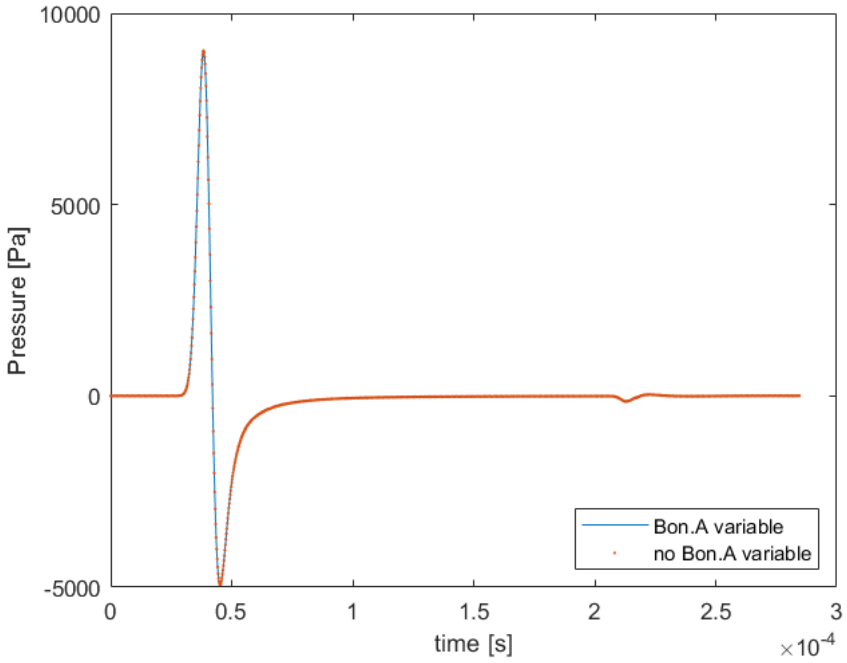

Figure 2. A comparison between simulations when using the Bon.A variable vs without. The simulation uses 20 cGy/pulse dose per pulse with a 4 μs pulsewidth.

For the propagation of the photoacoustic waves, they can be described through the thermoacoustic wave equation[37]:

$$\nabla^2 p(\vec{r},t) - \frac{1}{{v_s}^2}\frac{\partial^2}{\partial t^2}p(\vec{r},t) = -\frac{\beta}{C_p}\frac{\partial}{\partial t}H(\vec{r},t),$$

where $H(\vec{r},t)$ is the heat deposition at point $\vec{r}$ and time t, v_s is the speed of sound in medium, β is 160 the thermal expansion coefficient, and Cp is the specific heat capacity[78]. The pressure wave equation can be simplified by assuming that each individual proton pulse deposits the heat energy instantaneously. Thus, the protoacoustic measurement will ultimately reveal the proton Bragg peak (BP) location during dose delivery and the dose amount deposited to the target volume, which can be reconstructed through the use of

tomographic reconstruction algorithms. The workflow of this experimentally is described in Figure 3.

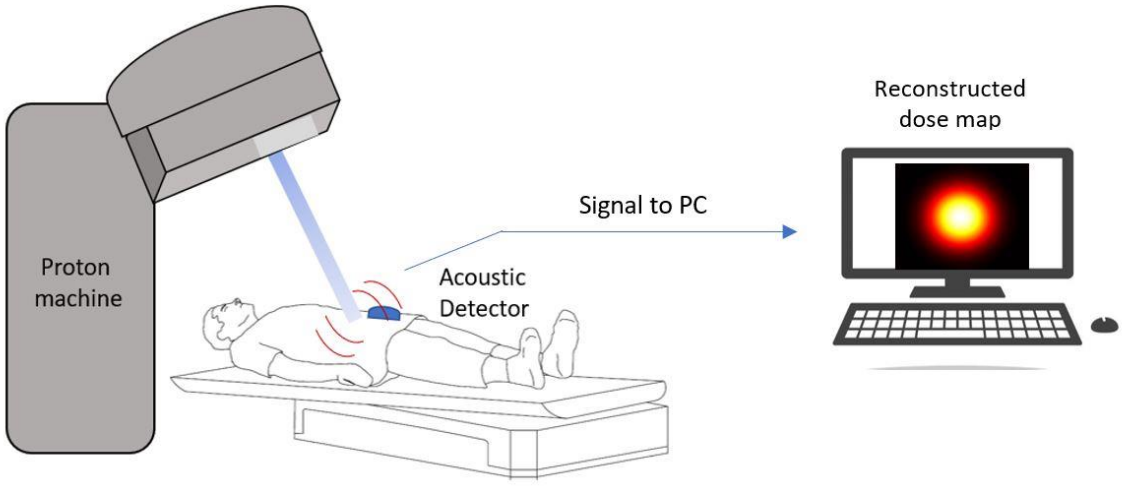

Figure 3. Basic workflow behind protoacoustics in FLASH proton therapy. The clinical pencil beam system irradiates the target with the greatest amount of energy being deposited at the Bragg peak. This irradiation generates acoustic pressure waves, which are detected by the acoustic detector. The detected pressure wave signals are then sent to the PC for further reconstruction and processing.

Simulation 1.

The first set of simulations completed was completed to observe the relationship between dose per pulse and the change in maximum amplitude. Dose per pulse was varied between 0.2 – 20 cGy/pulse while pulsewidth was kept consistent for each variation at 4 us. For each of the convolutions, the same Gaussian pulse shape was used. Simulations were completed in 3D using a 0.5 mm resolution and a 200 MeV proton beam, which was simulated using TOPAS. For the detector, a 5 x 5 cm 16 x 16 grid planar array was used and placed 5 cm past

the center of the Bragg peak. Next, to make the results of the simulation more realistic to experimental results, noise was added to the signals. The noise was added using the 'awgn' function in MATLAB. This function adds white noise depending on the simulated protoacoustic signal strength, which is proportional to dose per pulse. 5 dB noise was added based on several different experimental procedures. During proton therapy, electromagnetic background noise can be generated as well as proton beam spilling or other electrical noises (i.e. external devices). Using shielding for cables and signal filtering, a lot of this background noise can be reduced, leading to little-to-no fluctuation in the linearity of the signal. In the experimental and simulation papers related to specifically protoacoustics, SNR was calculated to be roughly 5 dB for single pulse acquisitions[65]. Another paper dealing exclusively with simulation set their SNR between 5 dB – 30 dB, which was also concluded based on other reports[70]. Due to this, the noise for the simulations done in this work are thoroughly justified.

Simulation 2

For the next set of simulations, rather than varying the dose per pulse, the pulsewidth in relation to the maximum amplitude of the signal was observed. The pulsewidths used were varied between 0.1 – 20 μs using a constant dose rate of 5 cGy/pulse. When determining the pulsewidths to use, it was ensured that they would fit within the thermal confinement using the thermal relaxation equation:

$$T_{th} = \frac{{d_c}^2}{4D_T}, \qquad (3)$$

Where the variable 'd_c' is the desired spatial resolution and 'DT' is the thermal diffusivity. For the calculations, a 'D_T' value of $\sim 0.114 \frac{mm^2}{sec}$ was used, which is the value of soft tissue, while

the d_c was assumed as around 1 mm, which is the smallest beam size used for the simulations[38]. As done in the first set of simulations, the same dimensions were used for the planar array detector with the 200 MeV proton beam. The pulsewidth was varied using a Gaussian pulse, which was convoluted with the generated acoustic pressure signal. To produce this pulse shape, the following Gaussian pulse was used:

$$G(t) = \frac{1}{\sigma\sqrt{2\pi}} exp\left(-\frac{1}{2}\frac{(t-\mu)^2}{\sigma^2}\right), \qquad (4)$$

Where μ is the position of the center of the pulse and σ is the Gaussian RMS width.

Simulation 3.

For the next set of simulations, reconstructions were completed for the simulations done with the varied pulsewidths. 2D time-reversal reconstructions were completed with a circular detector of 3 cm radius and 128 detector points. This detector was placed concentric to the BP volume and in the BP plane. This particular layout of the detector mimics the ring array detector that is used in the lab and is beneficial in obtaining a full view of the beam around. Figure 4 provides an image of the layout for the simulation setup. The sampling frequency that was used for this simulation was 20 MHz with the number of samples taken being 1415. The measurement data was generated using a grid with higher resolution (0.5 mm) and the time-reversal reconstructions used a courser grid (0.4 mm).

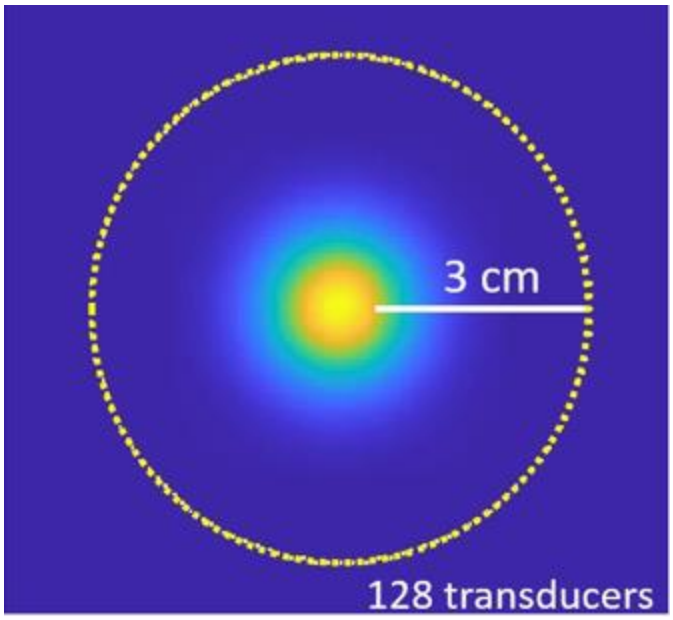

Figure 4. Demonstration of the layout for the simulation in k-Wave. The circular mask sensor used for the 2D reconstruction is displayed with the pressure source overlaid inside.

Simulation 4.

The next set of simulations takes a 150 MeV proton beam that was generated in TOPAS, similar to the other profiles. However, the biggest different with this simulation is that the beam is split into 9 beam spots, which were laid out into a 3 by 3 grid. This particular pattern was done to mimic spatially fractioned radiation therapy (SFRT). Using this newly made proton beam profile, 3D reconstructions were performed. An impulse heating pulse (δ-pulse) was assumed and the reconstructions used an 8 x 8 cm (16 x 16 elements) planar array, which was placed 5 cm behind the BP (Figure 5).

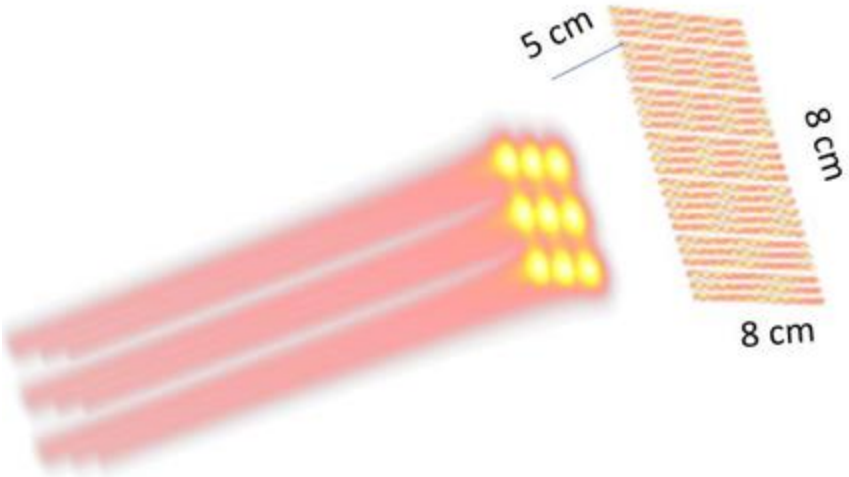

Figure 5. The layout of the 9 beamspot simulation in k-Wave. The planar array (8 cm x 8 cm) was used for the 3D reconstruction.

The reconstructions were performed for various pulsewidths: 1 μs, 2 μs, and 4 μs. Next, to characterize the reconstructions, Gaussian fitting was completed. This was done to then obtain the full width at half maximum (FWHM) as well as the peak reconstructed doses. The FWHM of the reconstructed beamlets from the fitted Gaussian RMS widths were evaluated using the following FWHM equation:

$$FWHM = 2\sqrt{2ln(2)}\sigma \tag{5}$$

CHAPTER 3: RESULTS AND DISCUSISON

With protoacoustics, one of the impressive characteristics is the linearity that can be observed between the dose and pressure signal. The purpose of the first set of simulations was to highlight this and determine if this linearity would continue to hold in the FLASH regime for proton therapy. The results from Figure 3 demonstrate the relationship between the varied dose between 0.2 – 20 cGy/pulse with the constant pulsewidth of 4 μs. Although 0.2 cGy/pulse is not considered FLASH, but rather, conventional dose rates, it was added into the simulations to demonstrate that linearity holds for both cases[79]. White Gaussian noise was added into this set of simulations as well at a value of 5 dB SNR to provide more realistic results. Multiple papers and reports for protoacoustic simulations use SNR values between 5 dB-30 dB, justifying the usage of these noise levels[65,70,80]. To view a better glimpse of the linearity between dose and pressure, Figure 3b provides a line of best fit across the maximum pressure of each dose based on the results of Figure 3a. The linear fit has an R2 value of 0.99. The results from these figures clearly show a linear response even as the dose per pulse increases to nearly 100 times greater than the dose per pulse that is achieved through current clinical machines. Many other dosimeters do display linearity, but there are no other published dosimeters that can achieve this with ultra-high dose rates. This is a feat that is shown through this simulation work. As mentioned in the previous section detailing various dosimeters, there are many difficulties with higher dose rates due to saturation. This problem is viewed even in the more popular dosimeters, such as ion chambers[25]. However, the works shown in the simulation clearly demonstrate the linearity. Although dose rates of between 0.2 – 20 cGy/pulse were shown, it's possible that lower or higher dose rates can be

used and show the same linearity trend. In fact, based on other completed works, it's highly possible that the dynamic range of protoacoustics is very large. Hickling et al.'s work demonstrates detection of doses as low as 11.6 mGy using XACT[81]. For higher doses, this has not yet been demonstrated experimentally as current clinical machines are not capable of this. The closest that this simulation can be compared to is the synchrocyclotron by Mevion, which has FLASH capabilities with a dose per pulse of 16 -32 cGy/pulse[82]. This range is high enough to produce FLASH proton energy, but is not strong enough to produce nonlinear effects.

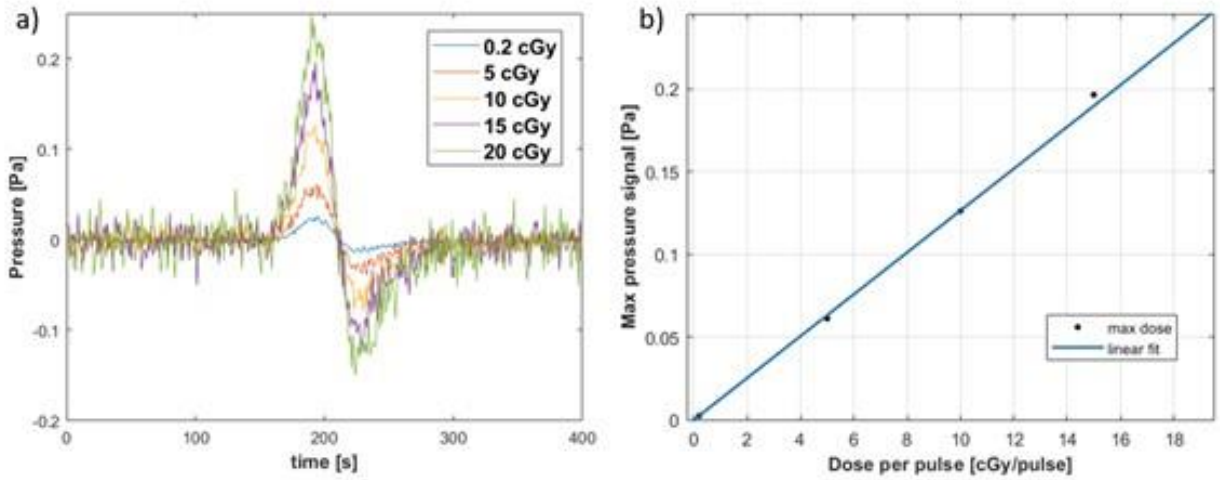

Figure 6. a) Protoacoustic signals simulated using k-Wave toolbox for dose per pulses varied between 0.2 cGy/pulse – 20 cGy/pulse with added white Gaussian noise. b) Relationship between the variation of the dose per pulse and the maximum pressure signal.

The second set of simulations completed in this work varied the pulsewidth to see the effects that it may have on the signal generation. To complete this, the resulting impulse protoacoustic signal was convoluted with the Gaussian pulse shape function. The protoacoustic signal from the center of the planar detector in the simulation was taken, and

the maximum value from the signals across the multiple pulsewidth variations were presented in Figure 4. The varied pulsewidths between 0.1 μs – 20 μs with a consistent 20 cGy/pulse is observed. Then, to see the resulting trend, Figure 4b plots the maximum amplitude of the protoacoustic signals with respect to the pulsewidths and is displayed with an exponential curve fit. The curve is fitted to the puslewidths larger than 1 μs with an R^2 value of 0.995. Ultimately, there is an increase in protoacoustic signal that can be viewed with the decrease in pulse duration. This is better viewed in Figure 4b, with the plot showing the relationship between the pulse amplitude and varied pulsewidths. The pulsewidths between 0.1 μs -1 μs show a plateau in the amplitude due to the satisfied stress confinement[83]. Because of this, the fitting for Figure 4b is only done with pulsewidths larger than 1 μs.

The next continuation of this simulation included 2D time-reversal reconstructions for each of the varied pulsewidths. The results of this is shown in Figure 4c, where a broadening effect is observed with increase of pulsewidth. Incidentally, this trend is also seen in the paper published by Sanbul et al, where 2D reconstructions were completed in a similar manner, but with a FLASH electron beam profile[84]. This broadening with the increase in pulsewidth could potentially lead to loss in the quantitative dose. To further identify and characterize this broadening in the reconstruction, future work will need to be completed.

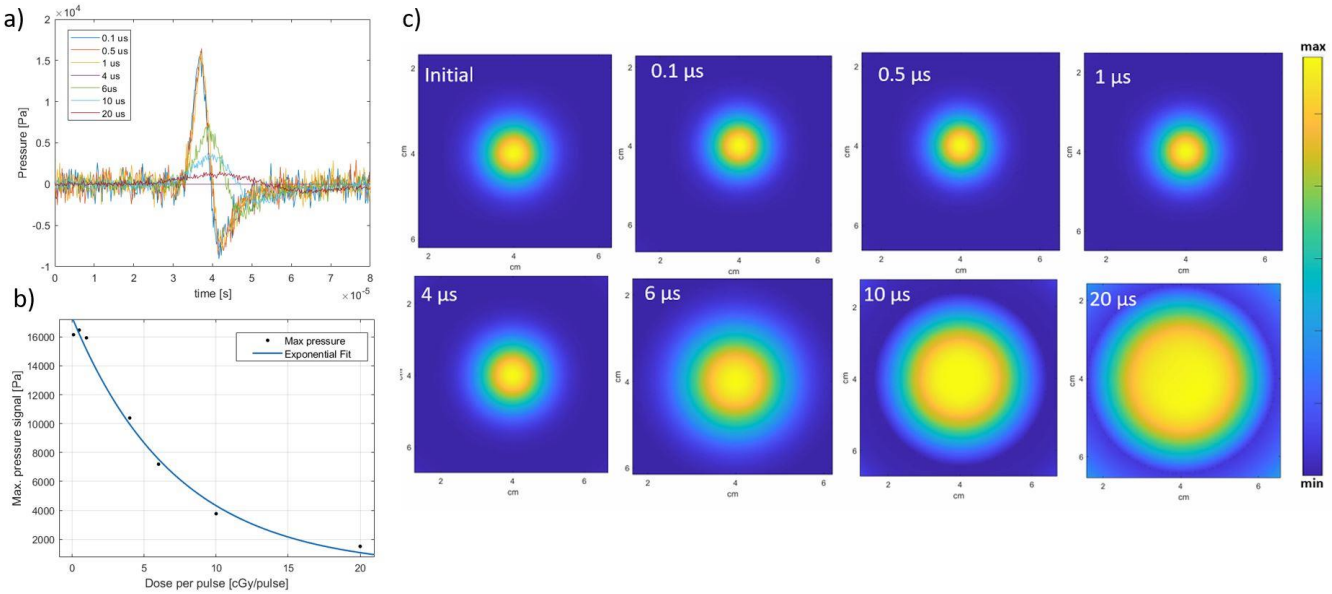

Figure 7a) Protoacoustic signals that were simulated using the k-Wave toolbox with varied pulsewidths and consistent dose per pulse. b) The relationship between signal amplitude and pulsewidth. An exponential curve fit was used to correlate the two past 1 µs. c) 2D reconstructions completed for the varied pulsewidths. The "initial" reconstruction is the incident beam to compare with the varied pulsewidths. Increase in beam size is seen with increasing pulsewidths.

The last set of simulations took the 150 MeV 9 beam spot profile, which was set into a 3 x 3 grid. This was completed to determine if visualization of each individual beamlet was possible through protoacoustic tomographic reconstruction. A clear image of the initial dose profile for this simulation can be found in Figure 5, where there is a 3D view and an XY slice image. The reconstruction of the BP plane slice corresponding to δ-pulse excitation is viewed in Figure 6a and the 3D render for the reconstructed dose maps are shown in Figure 6b. From the reconstructions, a broadening of the beam can be viewed as the pulsewidths increase, similar to the 2D case in the previous simulations.

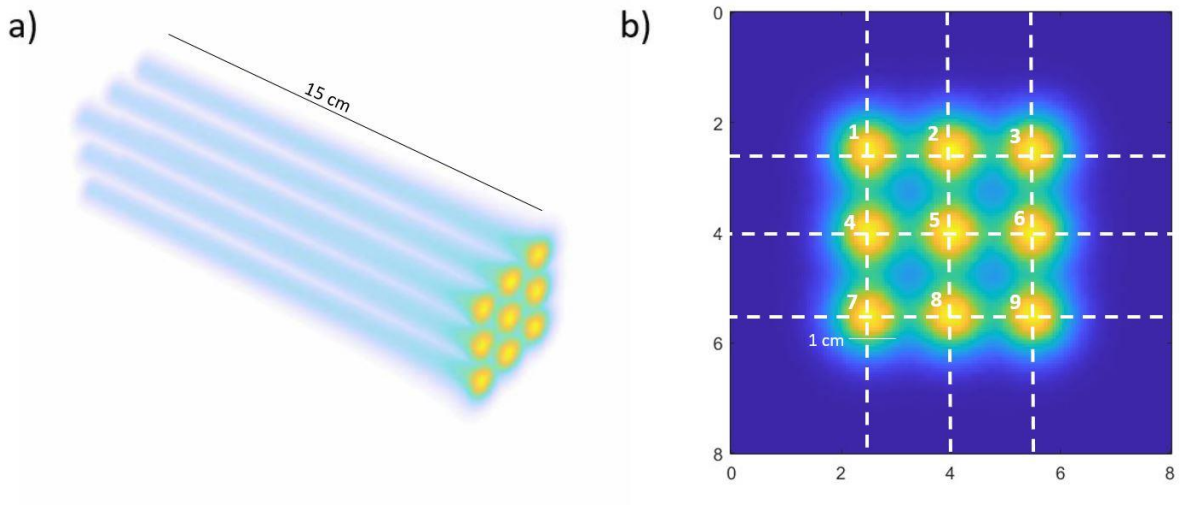

Figure 8. a) Initial dose deposition for the 150 MeV 9 beam spot file with the 1 cm beam spot size for beam. b) Initial dose deposition with a slice of the XY plane taken directly at the maximum dose of the 9 spot beam profile. The vertical and horizontal dotted lines across the figure represent where the FWHM was taken along.

To further analyze the results of the reconstructions, the FWHMs for each beamlet at the BP plane as well as the relative signal strengths are tabulated in Table 1. Based on the quantitative results, we were able to verify the pulsewidth-dependent broadening for the reconstructed beamlets. For the treatment and detection settings for this set of simulations, beamlets were not properly resolved for pulsewidths ≥ 4μs. To be able to resolve such large pulsewidths with smaller separations between each beamlet, a much larger transducer array aperture and smaller pitch would be needed. Another method of improving the results would be through deconvoluting the pulse function from the protoacoustic signals or through advanced reconstruction algorithms using finite pulsewidths.

This set of simulations employed 1 cm diameter beamlets to demonstrate LRT. The demonstration of protoacoustics on LRT is significant for multiple reasons. LRT is an

upcoming approach using an array of high dose regions. As it's been demonstrated clinically already, the potential for this technique to be more widely used, particularly on large tumor region is high. It's also a technique that many dosimeters are unable to perform 3D reconstruction on because a matrix array would be required for measurements or the system is only capable of point measurements. Many techniques are also limited in the sense that they are not capable of in vivo or real-time measurements, all characteristics that protoacoustics are capable of.

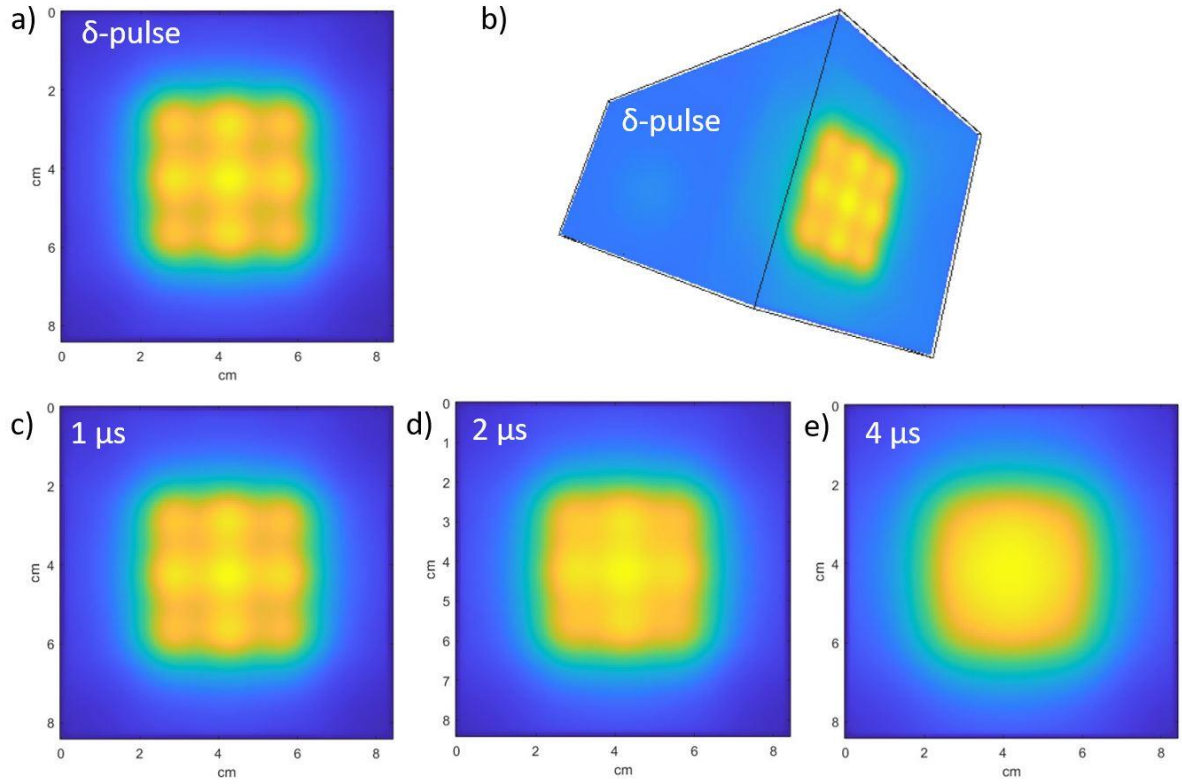

Figure 9a) XY slice from the 3D time-reversal δ-pulse reconstruction of the multi-beam proton deposition file at the center of the Bragg peak. b) 3D volumetric view of the reconstructed δ-pulse 9 beam file. Reconstructed XY slice at the Bragg peak for c) 1 μs, d) 2 μs, and e) 4 μs pulse durations.

Although protoacoustics does have its strengths in this particular simulation set, there are still slight setbacks that can be further investigated. The reconstruction for the study was completed with an 8 cm x 8 cm detector, where each individual beam was distinguishable from one another. Initially, a 5 cm x 5 cm planar array detector was used for the simulation. However, because the detector was too small, a proper image of each individual beamlet could not be resolved. In Table 1, the FWHM for each of the beam spots can be viewed, where the profiles along the horizontal and vertical lines as shown in Figure 5b were fitted to gaussians. The relative intensities of the beams were also obtained from the fitting and tabulated with the true values, which were all values taken from the simulated TOPAS energy deposition map. From the data taken in the table, it can be viewed that beam 5 has the most uniform angular coverage of the detector grid. This is also why the FWHM is expected to be the smallest and similar along the horizontal and vertical. Beamlets 1, 3, 7, and 9 are expected to have the largest FWHM values. Based on the symmetry of the problem, the horizontal and vertical FWHMs of both beams 2 and 8 are similar to the vertical and horizontal of beams 4 and 6.

Table 1. The FWHM and relative intensity values for each beam spot for Figure 9

Spot number	**Ground truth $FWHM_H$ (cm)**	**Reconstructed $FWHM_H$ (cm)**			**Ground truth $FWHM_V$ (cm)**	**Reconstructed $FWHM_V$ (cm)**			**Relative Intensities**		
		δ-pulse	1 μs PW	2 μs PW		δ - pulse	1 μs PW	2 μs PW	δ - pulse	1 μs PW	2 μs PW
1	1.14	1.65	1.75	1.78	1.11	1.64	1.72	1.76	0.83	0.86	0.88
2	1.10	1.38	1.41	1.80	1.09	1.63	1.73	1.78	0.95	0.94	0.95
3	1.19	1.71	1.78	1.84	1.13	1.67	1.75	1.77	0.83	0.85	0.86
4	1.14	1.68	1.77	1.81	1.16	1.44	1.45	1.78	0.95	0.94	0.95
5	1.11	1.39	1.41	1.74	1.16	1.39	1.42	1.77	1	1	1
6	1.14	1.71	1.79	1.86	1.13	1.42	1.44	1.80	0.95	0.92	0.93
7	1.09	1.64	1.76	1.79	1.13	1.67	1.76	1.86	0.83	0.85	0.86
8	1.19	1.42	1.42	1.77	1.11	1.71	1.78	1.84	0.95	0.92	0.93
9	1.08	1.73	1.80	1.87	1.13	1.72	1.78	1.85	0.83	0.83	0.85

CHAPTER 4: OUTLOOK

As an imaging modality, protoacoustics holds significant potential to transform the landscape of biomedicine, especially within cancer therapeutics. One of the possibilities for improvement is utilizing three-dimensional (3D) *in vivo* dosimetry through a 2D matrix array. This could provide greater precision in proton therapy by providing real-time monitoring and verification of radiation dose being delivered to the patient's tumor. In fact, this idea has been explored with the use of deep learning by Jiang et al. through deep learning tools[70]. A matrix array with 64 x 64 detectors was used and through simulation work, 3D pressure maps were generated. This study points towards a direction where real-time 3D dose verification in proton therapy can be possible. Although there are still limitations, such as lack of absolute dose as well as distortion and noise, these are each topics that can be addressed with further studies.

The concept of using a dual-modal imaging system can also be implemented in protoacoustics. There have been multiple studies conducted within photoacoustics (PA), which combines the use of medical imaging modalities with PA[85]. Such modalities include magnetic resonance imaging (MRI), x-ray computed tomography (CT), and ultrasound (US). The benefits of such a technique include the ability to also have structural information.

In particular, for the combination of PA with US, real-time imaging of both has been accomplished with a single handheld transducer probe[86]. This is possible as the mechanism for receiving the signal in both PA and US are the same, making the integration simple[87]. Similarly, this principle can be applied to protoacoustics and ultrasound to provide the protoacoustic signal alongside ultrasound information. In the clinic, such information would be valuable because the location of surrounding organs is not accurately seen as proton

radiation is being delivered to the patient. By being able to view in real-time the location of the proton Bragg peak overlaid onto the ultrasound, there would be greater accuracy and information during treatment. There have already been initial studies completed, which investigate co-registration of protoacoustics and ultrasound images[88]. In the results, the position of the Bragg peak was determined in the ultrasound image with submillimeter accuracy. However, there is still more studies that can be accomplished in this field. There is still a lack of studies that demonstrate this concept in real-time, and eventually, applying this technique to FLASH proton therapy would show great strides towards clinical applications. Furthermore, the integration of protoacoustic imaging and planning CT scans can become a valuable tool. The implementation of the planning CT scans could provide a way to correct the sound of speed in heterogeneous tissues, refining the accuracy of protoacoustic imaging. Currently, in many cases, a fully homogenous tissue is assumed. However, this is not the case if looking at animal or patient studies, where every layer will have a different sound speed. With pulse-echo ultrasound being integrated, real-time tumor motion tracking can be achieved, similar to how MRI is, which would enhance the adaptability and efficacy of proton therapy[53].

Although the innovation and improvements in protoacoustics has been drastic over the last several years, there are still many hurdles that need to be overcome before the technology reaches the clinic. When looking at the technical standpoint, the hardware for imaging systems still needs to be optimized to provide high-quality, real-time images for guided clinical decision making. Similarly, software algorithms used for image reconstruction and signal processing still need to be fine-tuned to handle complexities of real-world clinical data.

From the regulatory standpoint, there is still much to understand in the safety, efficacy, and reliability of protoacoustic imaging in the clinic. There's also costs that need to be considered in the development and implementation of the systems, which will need to be justified based on the improvement in patient outcome. When implementing the technology to FLASH specifically, there are even more hurdles, as the biological impact of FLASH has yet to be fully studied and understood. In the study by Lascaud and Parodi, multiple simulation studies were presented of acoustic cavitations that can occur during FLASH radiotherapy[89]. Based on their studies as well as others, it's possible that FLASH and such high intensity therapies could be enough to cause severe injuries[90]. Ultimately, more work should be completed on every aspect for protoacoustics prior to its introduction into clinical studies.

CHAPTER 5: CONCLUSION

The work that has been presented demonstrates the potential for protoacoustics in proton FLASH therapy through simulation studies. By utilizing the principles of radiation acoustics for imaging purposes, benefits such as non-invasive and *in vivo* measurements can be accomplished.

Through the simulations, parameters important to FLASH proton therapy, such as the dose per pulse and pulsewidth, were varied to match the clinical characteristics. Clinical energy proton beams were also used in the study. Through variation of dose per pulse, a wide dynamic range was demonstrated for protoacoustics while continuing to maintain linearity in the acoustic pressure of the protoacoustic signal. Pulsewidth was also varied through the simulation work and 2D reconstructions were performed to understand the effects the parameter has on signal generation and the proton beam itself. For the reconstructions, an increase was viewed in the beam diameter with increasing pulsewidth. The 3D reconstruction for beam geometries for LRT were also demonstrated using an 8 cm x 8 cm planar array, with high visibility of each beam. The results of the work show potential for protoacoustics in the clinic because of its linearity even with FLASH parameters, which is difficult to see in many current dosimeters.

With the ongoing advancements in technology as well as the increasing clinical recognition of the benefits behind proton therapy, protoacoustic imaging remains as a promising modality. Future research should focus on addressing the current challenges, such as reconstruction limitations or investigating the full dynamic range of protoacoustics.

References

1. Siegel RL, Miller KD, Fuchs HE, Jemal A. Cancer statistics, 2022. *CA Cancer J Clin*. 2022;72(1):7-33. doi:10.3322/CAAC.21708

2. Gianfaldoni S, Gianfaldoni R, Wollina U, Lotti J, Tchernev G, Lotti T. An Overview on Radiotherapy: From Its History to Its Current Applications in Dermatology. *Open Access Maced J Med Sci*. 2017;5(4):521. doi:10.3889/OAMJMS.2017.122

3. Radiation Therapy for Cancer - NCI. Accessed May 10, 2024. https://www.cancer.gov/about-cancer/treatment/types/radiation-therapy

4. Liu H, Chang JY. Proton therapy in clinical practice. *Chin J Cancer*. 2011;30(5):315. doi:10.5732/CJC.010.10529

5. Malouff TD, Serago C, Trifiletti DM. A Brief History of Particle Radiotherapy. *Principles and Practice of Particle Therapy*. Published online January 1, 2022:1-9. doi:10.1002/9781119707530.CH1

6. Karube M, Nakayama H. Proton therapy for patients with esophageal cancer: History, characteristics, clinical outcome and future direction of proton beam therapy. *Glob Health Med*. 2021;3(3):149-156. doi:10.35772/GHM.2020.01083

7. de Kruijff RM. FLASH radiotherapy: ultra-high dose rates to spare healthy tissue. *Int J Radiat Biol*. 2020;96(4):419-423. doi:10.1080/09553002.2020.1704912

8. Favaudon V, Caplier L, Monceau V, et al. Ultrahigh dose-rate FLASH irradiation increases the differential response between normal and tumor tissue in mice. *Sci Transl Med*. 2014;6(245). doi:10.1126/SCITRANSLMED.3008973

9. Romano F, Bailat C, Jorge PG, Lerch MLF, Darafsheh A. Ultra-high dose rate dosimetry: Challenges and opportunities for FLASH radiation therapy. *Med Phys*. 2022;49(7):4912-4932. doi:10.1002/MP.15649

10. Kim MM, Darafsheh A, Schuemann J, et al. Development of Ultra-High Dose-Rate (FLASH) Particle Therapy. *IEEE Trans Radiat Plasma Med Sci*. 2022;6(3):252-262. doi:10.1109/TRPMS.2021.3091406

11. Singers Sørensen B, Krzysztof Sitarz M, Ankjærgaard C, et al. In vivo validation and tissue sparing factor for acute damage of pencil beam scanning proton FLASH. *Radiotherapy and Oncology*. 2022;167:109-115. doi:10.1016/J.RADONC.2021.12.022

12. Vozenin MC, Hendry JH, Limoli CL. Biological Benefits of Ultra-high Dose Rate FLASH Radiotherapy: Sleeping Beauty Awoken. *Clin Oncol (R Coll Radiol)*. 2019;31(7):407-415. doi:10.1016/J.CLON.2019.04.001

13. FLASH Radiation Therapy: Review of the Literature and Considerations for Future Research and Proton Therapy FLASH Trials | Applied Radiation Oncology. Accessed May 11, 2024.

https://www.appliedradiationoncology.com/articles/flash-radiation-therapy-review-of-the-literature-and-considerations-for-future-research-and-proton-therapy-flash-trials

14. Jolly S, Owen H, Schippers M, Welsch C. Technical challenges for FLASH proton therapy. *Phys Med*. 2020;78:71-82. doi:10.1016/J.EJMP.2020.08.005

15. Buonanno M, Grilj V, Brenner DJ. Biological effects in normal cells exposed to FLASH dose rate protons. *Radiotherapy and Oncology*. 2019;139:51-55. doi:10.1016/J.RADONC.2019.02.009

16. Girdhani S, Abel E, Katsis A, et al. Abstract LB-280: FLASH: A novel paradigm changing tumor irradiation platform that enhances therapeutic ratio by reducing normal tissue toxicity and activating immune pathways. *Cancer Res*. 2019;79(13_Supplement):LB-280. doi:10.1158/1538-7445.AM2019-LB-280

17. Yan W, Khan MK, Wu X, et al. Spatially fractionated radiation therapy: History, present and the future. *Clin Transl Radiat Oncol*. 2020;20:30-38. doi:10.1016/j.ctro.2019.10.004

18. Schneider T, Fernandez-Palomo C, Bertho A, et al. Combining FLASH and spatially fractionated radiation therapy: The best of both worlds. *Radiotherapy and Oncology*. 2022;175:169-177. doi:10.1016/J.RADONC.2022.08.004

19. Wu X, Perez NC, Zheng Y, et al. The Technical and Clinical Implementation of LATTICE Radiation Therapy (LRT). *https://doi.org/101667/RADE-20-000661*. 2020;194(6):737-746. doi:10.1667/RADE-20-00066.1

20. Ashraf MR, Rahman M, Zhang R, et al. Dosimetry for FLASH Radiotherapy: A Review of Tools and the Role of Radioluminescence and Cherenkov Emission. *Front Phys*. 2020;8:328. doi:10.3389/FPHY.2020.00328/BIBTEX

21. Bourhis J, Montay-Gruel P, Gonçalves Jorge P, et al. Clinical translation of FLASH radiotherapy: Why and how? *Radiother Oncol*. 2019;139:11-17. doi:10.1016/J.RADONC.2019.04.008

22. Schüler E, Trovati S, King G, et al. Experimental Platform for Ultra-high Dose Rate FLASH Irradiation of Small Animals Using a Clinical Linear Accelerator. *International Journal of Radiation Oncology*Biology*Physics*. 2017;97(1):195-203. doi:10.1016/J.IJROBP.2016.09.018

23. Eling L, Bouchet A, Nemoz C, et al. Ultra high dose rate Synchrotron Microbeam Radiation Therapy. Preclinical evidence in view of a clinical transfer. *Radiotherapy and Oncology*. 2019;139:56-61. doi:10.1016/J.RADONC.2019.06.030

24. Jorge PG, Jaccard M, Petersson K, et al. Dosimetric and preparation procedures for irradiating biological models with pulsed electron beam at ultra-high dose-rate. *Radiotherapy and Oncology*. 2019;139:34-39. doi:10.1016/J.RADONC.2019.05.004

25. McManus M, Romano F, Lee ND, et al. The challenge of ionisation chamber dosimetry in ultra-short pulsed high dose-rate Very High Energy Electron beams. *Sci Rep*. 2020;10(1). doi:10.1038/S41598-020-65819-Y

26. Romano F, Subiel A, McManus M, et al. Challenges in dosimetry of particle beams with ultra-high pulse dose rates. *J Phys Conf Ser*. 2020;1662(1):012028. doi:10.1088/1742-6596/1662/1/012028

27. Kranzer R, Poppinga D, Weidner J, et al. Ion collection efficiency of ionization chambers in ultra-high dose-per-pulse electron beams. *Med Phys*. 2021;48(2):819-830. doi:10.1002/MP.14620

28. O'Leary M, Boscolo D, Breslin N, et al. Observation of dose-rate dependence in a Fricke dosimeter irradiated at low dose rates with monoenergetic X-rays. *Scientific Reports 2018 8:1*. 2018;8(1):1-9. doi:10.1038/s41598-018-21813-z

29. Hayes RB, Haskell EH, Wieser A, Romanyukha AA, Hardy BL, Barrus JK. Assessment of an alanine EPR dosimetry technique with enhanced precision and accuracy. *Nucl Instrum Methods Phys Res A*. 2000;440(2):453-461. doi:10.1016/S0168-9002(99)00957-2

30. Cao Y, Wang S, Luo C. Uncertainties in alanine/ESR dosimetry at the Physikalisch-Technische Bundesanstalt. *Phys Med Biol*. 2006;51(21):5419. doi:10.1088/0031-9155/51/21/003

31. Siddique S, Ruda HE, Chow JCL. FLASH Radiotherapy and the Use of Radiation Dosimeters. *Cancers 2023, Vol 15, Page 3883*. 2023;15(15):3883. doi:10.3390/CANCERS15153883

32. Motta S, Christensen JB, Frei F, Peier P, Yukihara EG. Investigation of TL and OSL detectors in ultra-high dose rate electron beams. *Phys Med Biol*. 2023;68(14):145007. doi:10.1088/1361-6560/ACDFB2

33. Scintillation Dosimetry - Google Books. Accessed May 11, 2024. https://books.google.com/books?hl=en&lr=&id=UAjYCwAAQBAJ&oi=fnd&pg=PP1&ots=1skBBA0b0W&sig=Zz-1XM7E_rnSTCEsjyczhxL9ZTM#v=onepage&q&f=false

34. Beddar S, Archambault L, Sahoo N, et al. Exploration of the potential of liquid scintillators for real-time 3D dosimetry of intensity modulated proton beams. *Med Phys*. 2009;36(5):1736-1743. doi:10.1118/1.3117583

35. Emelianov SY, Li PC, O'Donnell M. Photoacoustics for molecular imaging and therapy. *Phys Today*. 2009;62(8):34. doi:10.1063/1.3141939

36. Lyamshev LM. Radiation acoustics. *Soviet Physics - Uspekhi*. 1992;35(4):43-94. doi:10.1070/PU1992V035N04ABEH002227/XML

37. Xu M, Wang L V. Photoacoustic imaging in biomedicine. *Review of Scientific Instruments*. 2006;77(4):041101. doi:10.1063/1.2195024

38. Xia J, Yao J, Wang L V. Photoacoustic tomography: principles and advances. *Electromagn Waves (Camb)*. 2014;147:1-22. doi:10.2528/PIER14032303

39. Beard P. Biomedical photoacoustic imaging. *Interface Focus*. 2011;1(4):602-631. doi:10.1098/RSFS.2011.0028

40. Laufer J. Photoacoustic imaging: Principles and applications. *Quantification of Biophysical Parameters in Medical Imaging*. Published online February 21, 2018:303-324. doi:10.1007/978-3-319-65924-4_13/FIGURES/14

41. Xiang L, Han B, Carpenter C, Pratx G, Kuang Y, Xing L. X-ray acoustic computed tomography with pulsed x-ray beam from a medical linear accelerator. *Med Phys*. 2013;40(1):010701. doi:10.1118/1.4771935

42. Hoelen CGA, de Mul FFM. A new theoretical approach to photoacoustic signal generation. *J Acoust Soc Am*. 1999;106(2):695-706. doi:10.1121/1.427087

43. Parodi K, Assmann W. Ionoacoustics: A new direct method for range verification. *Mod Phys Lett A*. 2015;30(17):1540025. doi:10.1142/S0217732315400258

44. Yu Y, Li Z, Zhang D, Xing L, Peng H. Simulation studies of time reversal-based protoacoustic reconstruction for range and dose verification in proton therapy. *Med Phys*. 2019;46(8):3649-3662. doi:10.1002/MP.13661

45. Sulak L, Armstrong T, Baranger H, et al. Experimental studies of the acoustic signature of proton beams traversing fluid media. *Nuclear Instruments and Methods*. 1979;161(2):203-217. doi:10.1016/0029-554X(79)90386-0

46. Smith AR. Vision : Proton therapy. *Med Phys*. 2009;36(2):556-568. doi:10.1118/1.3058485

47. Tada J, Hayakawa Y, Hosono K, Inada T. Time resolved properties of acoustic pulses generated in water and in soft tissue by pulsed proton beam irradiation—A possibility of doses distribution monitoring in proton radiation therapy. *Med Phys*. 1991;18(6):1100-1104. doi:10.1118/1.596618

48. Kellnberger S, Assmann W, Lehrack S, et al. Ionoacoustic tomography of the proton Bragg peak in combination with ultrasound and optoacoustic imaging. *Scientific Reports 2016 6:1*. 2016;6(1):1-7. doi:10.1038/srep29305

49. Ahmad M, Xiang L, Yousefi S, Xing L. Theoretical detection threshold of the proton-acoustic range verification technique. *Med Phys*. 2015;42(10):5735. doi:10.1118/1.4929939

50. Patch SK, Santiago-Gonzalez D, Mustapha B. Thermoacoustic range verification in the presence of acoustic heterogeneity and soundspeed errors – Robustness relative to ultrasound image of underlying anatomy. *Med Phys*. 2019;46(1):318-327. doi:10.1002/MP.13256

51. Lehrack S, Assmann W, Bertrand D, et al. Submillimeter ionoacoustic range determination for protons in water at a clinical synchrocyclotron. *Phys Med Biol*. 2017;62(17):L20. doi:10.1088/1361-6560/AA81F8

52. Assmann W, Kellnberger S, Reinhardt S, et al. Ionoacoustic characterization of the proton Bragg peak with submillimeter accuracy. *Med Phys*. 2015;42(2):567-574. doi:10.1118/1.4905047

53. Samant P, Trevisi LM, Chen Y, Zwart T, Xiang L. 3D Protoacoustic Imaging through a Planar Ultrasound Array: A Simulation Workflow. *IEEE Trans Radiat Plasma Med Sci*. Published online May 26, 2022:1-1. doi:10.1109/TRPMS.2022.3177236

54. Nie W, Jones KC, Petro S, Kassaee A, Sehgal CM, Avery S. Proton range verification in homogeneous materials through acoustic measurements. *Phys Med Biol*. 2018;63(2):025036. doi:10.1088/1361-6560/AA9C1F

55. Durante M, Paganetti H, Knopf AC, Lomax A. In vivo proton range verification: a review. *Phys Med Biol*. 2013;58(15):R131. doi:10.1088/0031-9155/58/15/R131

56. Sueyasu S, Takayanagi T, Miyazaki K, et al. Ionoacoustic application of an optical hydrophone to detect proton beam range in water. *Med Phys*. 2023;50(4):2438-2449. doi:10.1002/MP.16189

57. Assmann W, Kellnberger S, Reinhardt S, et al. Ionoacoustic characterization of the proton Bragg peak with submillimeter accuracy. *Med Phys*. 2015;42(2):567-574. doi:10.1118/1.4905047

58. Lascaud J, Kowalewski R, Wollant B, et al. Optimization of the backing material of a low frequency PVDF detector for ion beam monitoring during small animal proton irradiation. *IEEE International Ultrasonics Symposium, IUS*. Published online 2021. doi:10.1109/IUS52206.2021.9593703

59. Lascaud J, Kalunga R, Lehrack S, et al. Applicability of Capacitive Micromachined Ultrasonic Transducers for the detection of proton-induced thermoacoustic waves. *IEEE International Ultrasonics Symposium, IUS*. 2019;2019-October:143-146. doi:10.1109/ULTSYM.2019.8926023

60. Zhang W, Oraiqat I, Litzenberg D, et al. Real-time, volumetric imaging of radiation dose delivery deep into the liver during cancer treatment. *Nature Biotechnology 2023*. Published online January 2, 2023:1-8. doi:10.1038/s41587-022-01593-8

61. Bjegovic K, Sun L, Pandey PK, et al. 4D in vivo dosimetry for a FLASH electron beam using radiation-induced acoustic imaging. *Phys Med Biol*. Published online May 9, 2024. doi:10.1088/1361-6560/AD4950

62. Wang J, Sohn JJ, Lei Y, et al. Deep learning-based protoacoustic signal denoising for proton range verification. *Biomed Phys Eng Express*. 2023;9(4):045006. doi:10.1088/2057-1976/ACD257

63. Sohn J, Nie W, Avery S, et al. Wavelet-based protoacoustic signal denoising for proton range verification. *https://doi.org/101117/122550768*. 2020;11319(16):14-19. doi:10.1117/12.2550768

64. Vallicelli EA, Corona M, Dell'acqua M, Baschirotto A, Matteis M De. Denoising for Enhancing Signal-to-Noise Ratio in Proton Sound Detectors. *BioCAS 2021 - IEEE Biomedical Circuits and Systems Conference, Proceedings*. Published online 2021. doi:10.1109/BIOCAS49922.2021.9644987

65. Caron J, Gonzalez G, Pandey PK, et al. Single pulse protoacoustic range verification using a clinical synchrocyclotron. *Phys Med Biol*. 2023;68(4):045011. doi:10.1088/1361-6560/ACB2AE

66. Xu M, Wang L V. Universal back-projection algorithm for photoacoustic computed tomography. *Phys Rev E Stat Nonlin Soft Matter Phys*. 2005;71(1):016706. doi:10.1103/PHYSREVE.71.016706/FIGURES/5/MEDIUM

67. Kellnberger S, Assmann W, Lehrack S, et al. Ionoacoustic tomography of the proton Bragg peak in combination with ultrasound and optoacoustic imaging. *Scientific Reports 2016 6:1*. 2016;6(1):1-7. doi:10.1038/srep29305

68. Van Dongen KWA, De Blécourt AJ, Lens E, Schaart DR, Vos FM. Reconstructing 3D proton dose distribution using ionoacoustics. *Phys Med Biol*. 2019;64(22):225005. doi:10.1088/1361-6560/AB4CD5

69. Mast TD, Johnstone DA, Dumoulin CL, Lamba MA, Patch SK. Reconstruction of thermoacoustic emission sources induced by proton irradiation using numerical time reversal. *Phys Med Biol*. 2023;68(2):025003. doi:10.1088/1361-6560/ACABFC

70. Jiang Z, Sun L, Yao W, Wu QJ, Xiang L, Ren L. 3D in vivo dose verification in prostate proton therapy with deep learning-based proton-acoustic imaging. *Phys Med Biol*. 2022;67(21):215012. doi:10.1088/1361-6560/AC9881

71. Faddegon B, Ramos-Méndez J, Schuemann J, et al. The TOPAS tool for particle simulation, a Monte Carlo simulation tool for physics, biology and clinical research. *Physica Medica*. 2020;72:114-121. doi:10.1016/J.EJMP.2020.03.019

72. Lee H, Cheon BW, Feld JW, et al. TOPAS-imaging: Extensions to the TOPAS simulation toolkit for medical imaging systems. *Phys Med Biol*. 2023;68(8). doi:10.1088/1361-6560/ACC565

73. Yao DK, Zhang C, Maslov KI, Wang L V. Photoacoustic measurement of the Grüneisen parameter of tissue. *https://doi.org/101117/1JBO191017007*. 2014;19(1):017007. doi:10.1117/1.JBO.19.1.017007

74. Treeby BE, Cox BT. k-Wave: MATLAB toolbox for the simulation and reconstruction of photoacoustic wave fields. *https://doi.org/101117/13360308*. 2010;15(2):021314. doi:10.1117/1.3360308

75. Hepler LG. Thermal expansion and structure in water and aqueous solutions. *https://doi.org/101139/v69-762*. 2011;47(24):4613-4617. doi:10.1139/V69-762

76. Petrova E, Ermilov S, Su R, Nadvoretskiy V, Conjusteau A, Oraevsky A. Using optoacoustic imaging for measuring the temperature dependence of Grüneisen parameter in optically absorbing solutions. *Opt Express*. 2013;21(21):25077. doi:10.1364/OE.21.025077

77. Slezak C, Flatscher J, Slezak P. A Comparative Feasibility Study for Transcranial Extracorporeal Shock Wave Therapy. *Biomedicines 2022, Vol 10, Page 1457*. 2022;10(6):1457. doi:10.3390/BIOMEDICINES10061457

78. Hickling S, Xiang L, Jones KC, et al. Ionizing radiation-induced acoustics for radiotherapy and diagnostic radiology applications. *Med Phys*. 2018;45(7):e707-e721. doi:10.1002/MP.12929

79. Scampoli P, Carpentieri C, Giannelli M, et al. Radiobiological characterization of the very high dose rate and dose per pulse electron beams produced by an IORT (intra operative radiation therapy) dedicated linac. *Transl Cancer Res*. 2017;6(S5):S761-S768. doi:10.21037/TCR.2017.05.21

80. Chino Y, Senoo Y, Kakinuma K, et al. 3D in vivo dose verification in prostate proton therapy with deep learning-based proton-acoustic imaging. *Phys Med Biol*. 2022;67(21):215012. doi:10.1088/1361-6560/AC9881

81. Hickling S, Hobson M, El Naqa I. Characterization of x-ray acoustic computed tomography for applications in radiotherapy dosimetry. *IEEE Trans Radiat Plasma Med Sci*. 2018;2(4):337-344. doi:10.1109/TRPMS.2018.2801724

82. Darafsheh A, Hao Y, Zwart T, et al. Feasibility of proton FLASH irradiation using a synchrocyclotron for preclinical studies. *Med Phys*. 2020;47(9):4348-4355. doi:10.1002/MP.14253

83. Jones KC, Seghal CM, Avery S. How proton pulse characteristics influence protoacoustic determination of proton-beam range: simulation studies. *Phys Med Biol*. 2016;61(6):2213-2242. doi:10.1088/0031-9155/61/6/2213

84. Ba Sunbul NH, Zhang W, Oraiqat I, et al. A simulation study of ionizing radiation acoustic imaging (iRAI) as a real-time dosimetric technique for ultra-high dose rate radiotherapy (UHDR-RT). *Med Phys*. 2021;48(10):6137-6151. doi:10.1002/MP.15188

85. Kim C, Chen Z. Multimodal photoacoustic imaging: systems, applications, and agents. *Biomed Eng Lett*. 2018;8(2):137-138. doi:10.1007/S13534-018-0071-6/METRICS

86. Kim J, Park S, Jung Y, et al. Programmable Real-time Clinical Photoacoustic and Ultrasound Imaging System. *Scientific Reports 2016 6:1*. 2016;6(1):1-11. doi:10.1038/srep35137

87. Kim C, Erpelding TN, Jankovic L, Wang L V. Performance benchmarks of an array-based hand-held photoacoustic probe adapted from a clinical ultrasound system for non-invasive sentinel lymph node imaging. *Philos Trans A Math Phys Eng Sci*. 2011;369(1955):4644. doi:10.1098/RSTA.2010.0353

88. Schauer J, Wieser HP, Lascaud J, et al. Range verification of a clinical proton beam in an abdominal phantom by co-registration of ionoacoustics and ultrasound. *Phys Med Biol*. 2023;68(12):125009. doi:10.1088/1361-6560/ACD834

89. Lascaud J, Parodi K. On the potential biological impact of radiation-induced acoustic emissions during ultra-high dose rate electron radiotherapy: a preliminary study. *Phys Med Biol*. 2023;68(5):05LT01. doi:10.1088/1361-6560/ACB9CE

90. Schwartz ML, Yeung R, Huang Y, et al. Skull bone marrow injury caused by MR-guided focused ultrasound for cerebral functional procedures. *J Neurosurg*. 2018;130(3):758-762. doi:10.3171/2017.11.JNS17968